Romanian Journal of Petroleum & Gas Technology
VOL. IV (LXXV) • No. 1/2023

INFLUENCE OF DIMENSIONLESS WELLBORE RADIUS ON DIMENSIONLESS PRESSURE AND PRESSURE DERIVATIVES

Patrick Ebelechukwu Akuagwu [1]

Wilfred Chinedu Okologume [1]

[1] Department of Petroleum Engineering, Federal University of Petroleum Resources, Effurun, Nigeria
e-mail: okologume.wilfred@fupre.edu.ng

DOI: 10.51865/JPGT.2023.01.07

ABSTRACT

Effects of wellbore radius on pressure derivatives of a vertical oil well is a major concern to oil and gas industry operators who intend to execute fluid production from a vertical oil well. Reservoir deliverability depends on several factors: the dimensionless wellbore radius. This study examines the influence of the dimensionless wellbore radius on the pressure and pressure derivative. A set of polynomials was implemented to calculate the dimensionless pressure variable and the pressure derivative. The polynomials were put into a computer program developed in the study to create a fast means through which the effect of wellbore radii can be studied easily. However, when several dimensionless radii were used as input parameters for the developed computer program, it was observed that the lower the dimensionless wellbore pressure, the higher the pressure derivative and vice versa. Also, lower dimensionless time yielded higher values of the dimensionless pressure variable. Results from the developed computer model were validated by comparing results from the model to those obtained from a published article while using the same input parameters (t_D and r_{WD}). Moreover, the percentage error was estimated to be less than 0.02%.

Keywords: wellbore, radius, dimensionless, pressure, derivatives

INTRODUCTION

Operators in the oil and gas industry who plan to carry out fluid production from a vertical oil well are extremely concerned about the implications of wellbore radius on the pressure derivatives of a vertical oil well. The difficulties associated with using conventional well test methods have been completely overcome by the use of dimensionless pressure and dimensionless pressure derivative type curves, leading to significant advancements in the analysis of well tests [1]. On the derivative plot, heterogeneities that are hardly perceptible on the traditional plot of well testing data are magnified. Similarly, using the derivative plot, flow regimes exhibit distinct and unambiguous outlines [2]. Water coning is largely caused by well production pressure gradients from the pay zone well. Water coning has been regarded as the main challenge during production from an oil reservoir with bottom water [3]. In horizontal wells, water coning is the factor that determines how much of an increase in production rate is permissible [4]. Rising water-cut negatively influences inflow performance and the tubing performance curve [5]. Wellbore pressure losses during horizontal well production increase the likelihood of conning in the later stages, making some of the horizontal well unproductive [6].

Adewole and Olafuyi [7] used the source and green functions to derive different dimensionless pressure and pressure derivatives for different directions of flow in an "A-shaped" architecture experiencing bottom water and concluded that individual layer characterization requires properties from only the layer involved, while comprehensive reservoir characterization requires equivalent (total layers) properties. Eiroboyi and Adewole [8] developed type curves for a reservoir with bottom water drive using source and green functions. The dimensionless wellbore response and its derivative at early radial flow were calculated using the standard pressure derivative formula proposed by Edobhiye and Adewole [9]. Moreover, they concluded that it is possible to investigate the effects of reservoir and wellbore properties on the dimensionless pressure and dimensionless pressure derivatives distribution of a horizontal well in a reservoir subject to gas cap, edge water, and bottom water drive mechanisms.

In previous research regarding dimensionless pressure and pressure derivatives, as presented in literature, numerical integration was used to compute P_D and P'_D. However, this procedure is often complex and difficult to use near the origin because of the asymptotic nature of the functions involved. Thus, this study employed a simpler approach using a set of polynomials that were easier to implement than numerical methods. More so, in a bid to apply these equations (polynomials) in calculating pressure derivatives for various dimensionless radii, this study developed a computer program. Furthermore, the computer program made it easy to investigate the influence of dimensionless wellbore radius on pressure derivatives, which was the major objective of this study. Therefore, this study seeks to study how wellbore radius influences the behaviour of dimensionless pressure and its derivative.

METHODOLOGY

Crossover point t_{cross}

The crossover point at a particular dimensionless radius is referred to as the dimensionless time (t_D) at which boundary effects are felt. The choice between using the finite or infinite set of polynomials to calculate P_D can be made once this crossover value of t_D has been established because the finite polynomials do not provide reliable results for values of t_D below this crossover point (t_{cross}). By examining the intersection points of infinite and finite P_D curve fits and using regression analysis, the value of t_D at which boundary effects are exhibited was estimated from Eq. 1 and Eq. 2.

$$t_{cross} = 0.0980958(r_D - 1) + 0.100683(r_D - 1)^{2.03863} \tag{1}$$

For values of $t_D < t_{cross}$, the aquifer is infinite-acting; thus, the infinite-aquifer approach discussed in subsequent sections should be used. If otherwise, that is $t_D \geq t_{cross}$, then the polynomial for finitely-acting aquifer would be used. More so, dimensionless time is calculated as follows:

$$t_D = \frac{2.309kt}{\mu\varphi c_t r_o^2} \tag{2}$$

Where t = time in years, μ =viscosity, c_t=total compressibility, φ =porosity and r_o= reservoir outer radius.

Determination of dimensionless pressure, P_D

a) Finite aquifers: Van Everdingen and Hurst model [10] is given by Eq. 11:

$$P(t_D) = \frac{2}{r_D^2-1}\left(\frac{1}{4}+t_D\right) - \frac{3r_D^4-4r_D^4\log_e r_D-2r_D^2-1}{4\left(r_D^2-1\right)^2} + 2\sum_{n=1}^{\infty}\frac{e^{-\beta_n^2 t_D}J_1^2(\beta_n r_D)}{\beta_n^2\left[j_1^2(\beta_n r_D)-j_1^2(\beta_n)\right]} \quad (3)$$

Where,

t_D = dimensionless time and is shown in Eq. 2,

r_D= the ratio of the aquifer radius to the reservoir radius (r_e/r_w) and

J_1 refers to the Bessel function of order 1.

While β defines the roots of the following equation.

$$J_1(\beta_n r_D)Y_1\left(\beta_n - J_1\beta_n Y_1(\beta_n r_D)\right) = 0 \quad (4)$$

Where J_1 and Y_1 are Bessel functions of order 1.

However, Eq. 3 was expressed in a polynomial form as follows;

$$P_D = \frac{2}{r_D^2-1}\left(\frac{1}{4}+t_D\right) - \frac{3r_D^4-4r_D^4\log_e r_D-2r_D^2-1}{4\left(r_D^2-1\right)^2} + \frac{2e^{-\beta_1^2 t_D}J_1^2(\beta_1 r_D)}{\beta_1^2\left[j_1^2(\beta_1 r_D)-j_1^2(\beta_1)\right]} + \frac{2e^{-\beta_2^2 t_D}J_1^2(\beta_2 r_D)}{\beta_2^2\left[j_1^2(\beta_2 r_D)-j_1^2(\beta_2)\right]} \quad (5)$$

Where,

$$\beta_1 = -0.00870415 - 1.08984\,\text{csch}(r_D) + 12.4458(r_D)^{-2.8446} + 3.4234(r_D)^{-0.949162} \quad (6)$$

$$\beta_2 = -0.0191642 - 2.47644\,\text{csch}(r_D) + 25.3343(r_D)^{-2.73054} + 6.13184(r_D)^{-0.939529} \quad (7)$$

csch(x) refers to the hyperbolic cosecant function which is computed as follows;

$$\text{csch}(x) = \frac{1}{e^x-e^{-x}} \quad (8)$$

Also, the first order Bessel functions were computed as shown in Eq. 9 and Eq. 10 below;

At condition: $0 \leq x < 3.0$

$$J_1(x) = \left[0.5 - 0.56249985\left(\frac{x}{3}\right)^2 + 0.21093573\left(\frac{x}{3}\right)^4 - 0.03954289\left(\frac{x}{3}\right)^6 + 0.00443319\left(\frac{x}{3}\right)^8 - 0.00031761\left(\frac{x}{3}\right)^{10} + 0.00001109\left(\frac{x}{3}\right)^{12}\right]x \quad (9)$$

At condition: $3.0 \leq x < \infty$

$$J_1(x) = (x)^{-0.5}F_1(\cos\theta_1) \quad (10)$$

$$F_1 = b_0 + b_1\left(\frac{3}{x}\right) + b_2\left(\frac{3}{x}\right)^2 + b_3\left(\frac{3}{x}\right)^3 + b_4\left(\frac{3}{x}\right)^4 + b_5\left(\frac{3}{x}\right)^5 + b_6\left(\frac{3}{x}\right)^6$$

b_o = 0.79788456, b_l = 0.00000156, b_2 = 0.01659667, b_3 = 0.00017105,

b_4 = -0.00249511, b_s = 0.00113653, and b_6 = -0.00020033.

$$\theta_1 = x - 2.35619449 + 0.12499612\left(\frac{3}{x}\right) + 0.00005650\left(\frac{3}{x}\right)^2 - 0.00637879\left(\frac{3}{x}\right)^3 + 0.00074348\left(\frac{3}{x}\right)^4 + 0.0079824\left(\frac{3}{x}\right)^5 - 0.00029166\left(\frac{3}{x}\right)^6$$

b) For Infinitely – acting aquifers:

For infinite aquifers, the value of P_D as a function of dimensionless time was determined using the Van Everdingen and Hurst model [10] as follows:

$$P_D = \frac{4}{\pi^2}\int_0^\infty \frac{\left(1-e^{-u^2 t_D}\right)du}{u^3\left[J_1^2(u)+Y_1^2(u)\right]} \tag{11}$$

An analytical solution to this integral was not available, and numerical methods were difficult to use near the origin because of the asymptotic nature of the function. Thus, for evaluation, the integral was broken into two parts such that Eq. 11 becomes,

$$P_D = \frac{4}{\pi^2}\int_0^\delta \frac{\left(1-e^{-u^2 t_D}\right)du}{u^3\left[J_1^2(u)+Y_1^2(u)\right]} + \frac{4}{\pi^2}\int_0^\infty \frac{\left(1-e^{-u^2 t_D}\right)du}{u^3\left[J_1^2(u)+Y_1^2(u)\right]} \tag{12}$$

Eq. 12 was solved analytically using non-linear regression to obtain a set of polynomial as shown in the following subsequent equations:

Condition: At $t_D \le 0.01$,

$$P_D = \frac{2}{\pi}\sqrt{t_D} \tag{13}$$

Condition: At $0.01 \le t_D < 500$,

$$P_D = \frac{1107.5868(t_D)^{0.5003552}+37.60613\mathrm{t_D}+7.038188(t_D)^{1.338479}}{95.13748+77.0034(t_D)^{0.5003552}+16.63856(t_D)+(t_D)^{1.338479}} \tag{14}$$

Condition: At $500 \le t_D$,

$$P_D = \frac{1}{2}[\log_e t_D]\left(1+\frac{1}{2t_D}\right) + 0.40454\left(1+\frac{1}{2t_D}\right) \tag{15}$$

Determination of pressure derivative, P'_D

a) Finite aquifers: Condition: $t_{cross} \le t_D$

$$P'_{\mathrm{D}} = \frac{2}{r_D^2-1} - \frac{2e^{-\beta_1^2 t_D} J_1^2(\beta_1 r_D)}{j_1^2(\beta_1 r_D)-j_1^2(\beta_1)} - \frac{2e^{-\beta_2^2 t_D} J_1^2(\beta_2 r_D)}{j_1^2(\beta_2 r_D)-j_1^2(\beta_2)} \tag{16}$$

b) Infinite aquifers:

Condition 1: $t_D \le 0.01$

$$P'_{\mathrm{D}} = \frac{1}{\sqrt{\pi t_D}} \tag{17}$$

Condition 2: $0.01 \le t_D < 500$

$$P'_{\mathrm{D}} = \frac{b_0+b_1(t_D)^{b_6}+b_2(t_D)^{b_7}+b_3(t_D)^{b_8}+b_4(t_D)^{b_9}+b_5(t_D)^{b_{10}}}{b_{11}+b_{12}(t_D)^{b_7}+b_{13}(t_D)+(t_D)^{b_9}} \tag{18}$$

Where,

$b_0 = 3577.752441$; $b_1 = 5121.404179$; $b_2 = 552.462473$; $b_3 = 364.062209$;

$b_4 = 26.908805$; $b_5 = 896.239475$; $b_6 = -0.499645$; $b_7 = 0.5003552$; $b_8 = 0.838834$;

b_9 = 1.338479; b_{10} = 0.338479; b_{11} = 95.13748; b_{12} = 77.0034; b_{13} = 16.63856.

Condition 3: $500 \leq t_D$

$$P'_D = \frac{1}{2t_D}\left[1 - \frac{\log_e(t_D)}{2t_D} + \frac{0.09546}{t_D}\right] \tag{20}$$

Computer model (EXPLORE)

The computer model (EXPLORE) developed in this study is a reservoir investigative toolkit for examining the influence of dimensionless wellbore radius (r_{WD}) on dimensionless pressure and pressure derivatives. The mathematical models discussed in the previous sections were incorporated into the developed toolkit "EXPLORE". The toolkit, however, was developed to decide the appropriate correlation/polynomial depending on the conditions of t_D and the cross-over point. The correlations to calculate pressure derivatives differ since the supposed aquifer may be acting finitely or infinitely. Furthermore, at a specified dimensionless time, t_D, boundary effects can either be felt or may not be felt (because the pressure disturbance has reached the boundary). Even so, the software is intelligent enough to know the two conditions. Also, the software present semi-log plots of pressure derivatives against dimensionless time for evaluation purposes. The software was developed using Microsoft Visual C#. The splash screen and the simplified flowchart of the developed software "EXPLORE" is shown in Fig.1 and Fig.2.

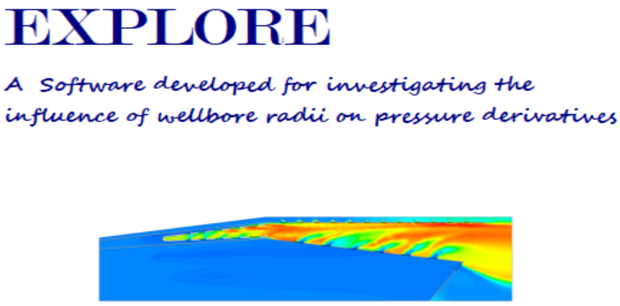

Fig. 1 *Software splash screen.*

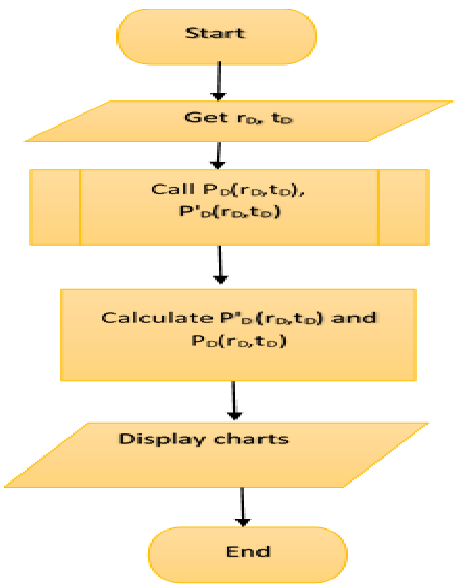

Fig. 2 *Flowchart for the developed computer model (EXPLORE)*

Computer model development

First, all necessary functions were created in a class. These functions include:

i. The hyperbolic cosecant function (csch(x))
ii. Bessel function of order 1 ($J_1(x)$)
iii. Dimensionless pressure function $P_D(r_{wD},t_D)$.
iv. Pressure derivative function $P'_D(r_{wD},t_D)$.

Assumptions made

The assumptions made for the mathematical models that were employed in the determination of dimensionless pressure and pressure derivatives are stated below;

i. The reservoir must be driven by an underground aquifer (i.e. a water drive reservoir with aquifer support)
ii. Calculations were made based on a vertical oil well and no geometry or location was considered.
iii. Dimensionless variables like dimensionless well bore radius, r_{WD}, and dimensionless time is known.
iv. A pseudo-steady state flow regime was assumed for either infinitely acting of finitely acting aquifers.

RESULTS AND DISCUSSION

Results from varying t_D at fixed r_{wD}

While using the developed toolkit (EXPLORE), a number of dimensionless time t_D, ranging from 0.001 to 10,000 were used as input parameter along with a fixed value of dimensionless wellbore radius (r_{wD}) of 0.01. The result is represented in a semi-logarithm chart as shown in Fig. 3. From the chart, it was observed that dimensionless pressure, P_D, increased exponentially from 0.02013 to 5.0. Meanwhile, pressure derivative was observed to have experienced a hyperbolic decrease from 17.84 to 4.9977E-05. This decrease however is reflective of the fact that pressure derivatives decrease at higher dimensionless time.

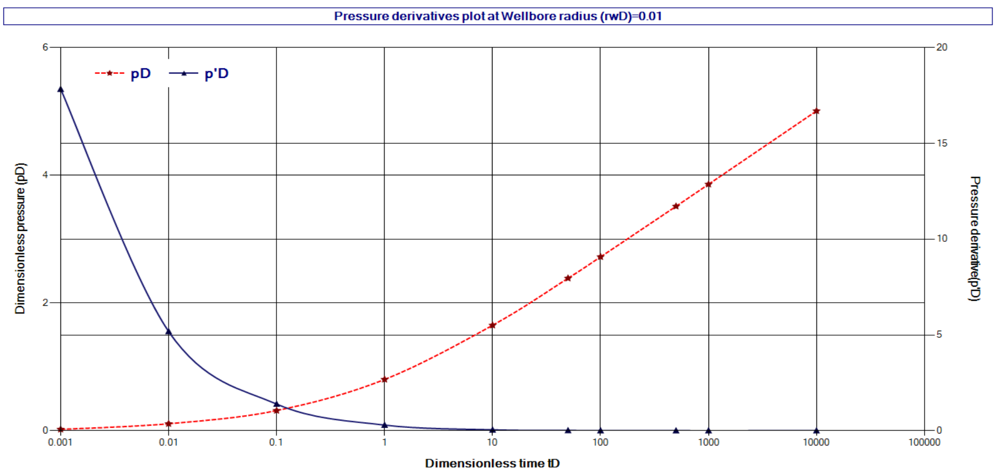

Fig. 3 *Dimensionless pressure and pressure derivative chart at r_{wD}=0.01*

Similarly, same procedure performed above was repeated for the following dimensionless wellbore radii: 5, 10, 20, 30, 50, 70 and 100. With a dimensionless radius of 5, dimensionless pressure P_D increased gradually and uniformly from 0.02013 (at t_D=0.01) to 9.31 (at t_D=100). Thereafter, there was a huge spike in P_D values at t_D =1000 and 10,000 respectively (see Fig. 4). This behaviour shows that P_D is very sensitive to dimensionless time. Conversely, pressure derivative (P'_D) decreased from 17.84 to 0.0833. It was also noticed that, from a dimensionless time of 10 and above, pressure derivative remained unchanged regardless of the increase in dimensionless time. Also, when the wellbore radius was adjusted to 10, the trend of the curve for dimensionless pressures against dimensionless time, remained same as that with a wellbore radius of 5.

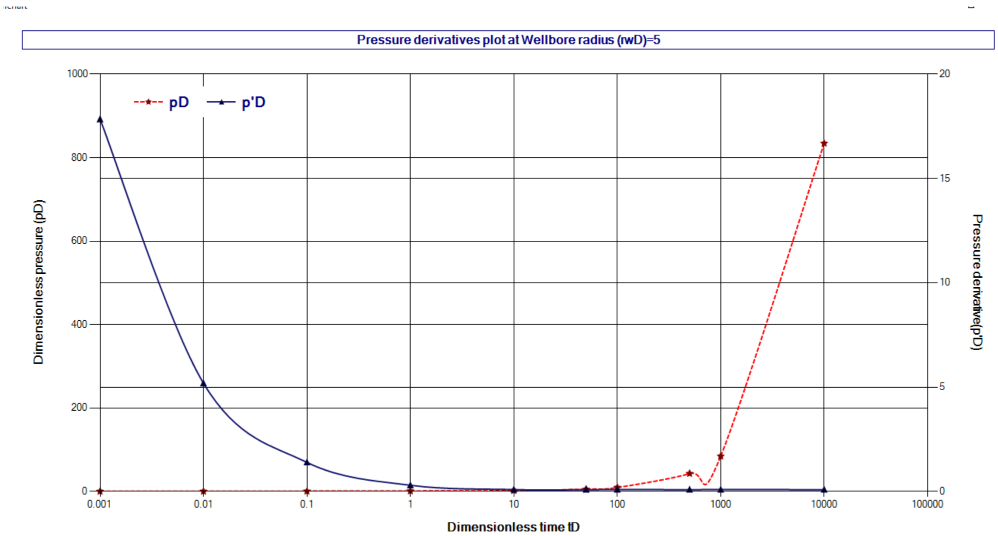

***Fig. 4** Dimensionless pressure and pressure derivative chart at r_{wD}=5*

Also, it was observed that the values of P_D became smaller when compared to P_D values at radius of 5. This is indicative of the fact that smaller wellbore radii often yield higher values of P_D. Same behaviour was observed for P'_D at r_{wD}=10 as seen in Fig. 5.

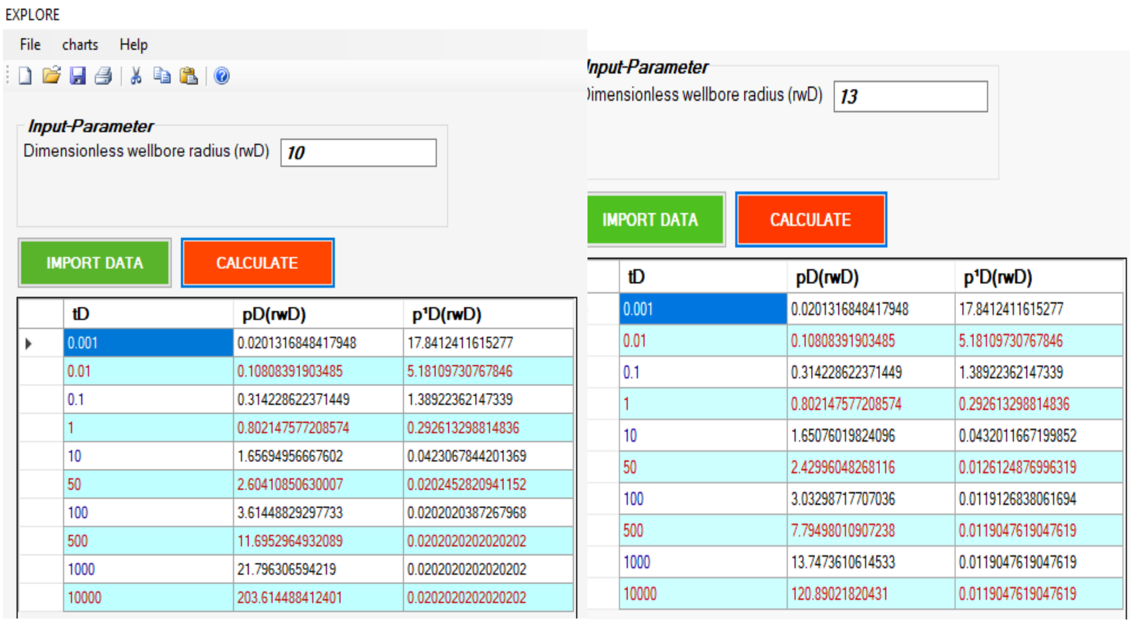

tD	pD(rwD)	p'D(rwD)
0.001	0.0201316848417948	17.8412411615277
0.01	0.10808391903485	5.18109730767846
0.1	0.314228622371449	1.38922362147339
1	0.802147577208574	0.292613298814836
10	1.65694956667602	0.0423067844201369
50	2.60410850630007	0.0202452820941152
100	3.61448829297733	0.0202020387267968
500	11.6952964932089	0.0202020202020202
1000	21.796306594219	0.0202020202020202
10000	203.614488412401	0.0202020202020202

tD	pD(rwD)	p'D(rwD)
0.001	0.0201316848417948	17.8412411615277
0.01	0.10808391903485	5.18109730767846
0.1	0.314228622371449	1.38922362147339
1	0.802147577208574	0.292613298814836
10	1.65076019824096	0.0432011667199852
50	2.42996048268116	0.0126124876996319
100	3.03298717707036	0.0119126838061694
500	7.79498010907238	0.0119047619047619
1000	13.7473610614533	0.0119047619047619
10000	120.89021820431	0.0119047619047619

***Fig. 5** Dimensionless pressure and pressure derivative calculations at r_{wD}=10 and at r_{wD}=13*

More so, the values of P'_D and P_D were observed to give same result for dimensionless times less than 5, regardless of the value of r_{wD}. Pressure derivatives at t_D=10 was estimated to be approximately 0.04231. But P'_D value maintained 0.0202 at dimensionless time greater than 10. The calculations of pressure derivatives at r_{wD}=13 is as represented in Fig. 5. The same result as that with r_{wD}=10 was obtained for dimensionless pressure (for t_D values less than 50) at r_{wD}=13. Moreover, the values of P_D were observed to have reduced in quantity when compared to those obtained at r_{wD}=10. This trend in data further justifies the fact that low wellbore dimensionless radius causes a corresponding increase in dimensionless pressure variable, P_D, and vice versa. The aforementioned assertion still holds for pressure derivative (P'_D).

At t_D values higher than 10, the values of pressure derivative remained constant. This shows that increasing dimensionless time to an exceedingly high value, will often have little to no effect on the underground aquifer influencing the oil reservoir. Furthermore, trying out wellbore radius of 20 and 30, the results obtained are illustrated in Fig. 6 and Fig. 7 respectively. The assertion that "high wellbore radius results in low pressure derivatives" still stands. Nevertheless, at a dimensionless wellbore radius of 50, a somewhat weird trend was observed for dimensionless pressure variable, P_D as shown in Fig. 8.

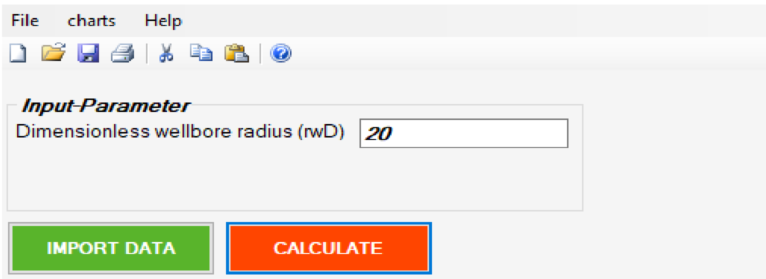

tD	pD(rwD)	p'D(rwD)
0.001	0.0201316848417948	17.8412411615277
0.01	0.10808391903485	5.18109730767846
0.1	0.314228622371449	1.38922362147339
1	0.802147577208574	0.292613298814836
10	1.65076019824096	0.0432011667199852
50	2.37390905688553	0.0101575046468904
100	2.739765423576	0.00579577807978635
500	4.76577981705922	0.00501253158900967
1000	7.27204548821074	0.0050125313283208
10000	52.384827443098	0.0050125313283208

Fig. 6 *Dimensionless pressure and pressure derivative calculations at r_{wD}=20*

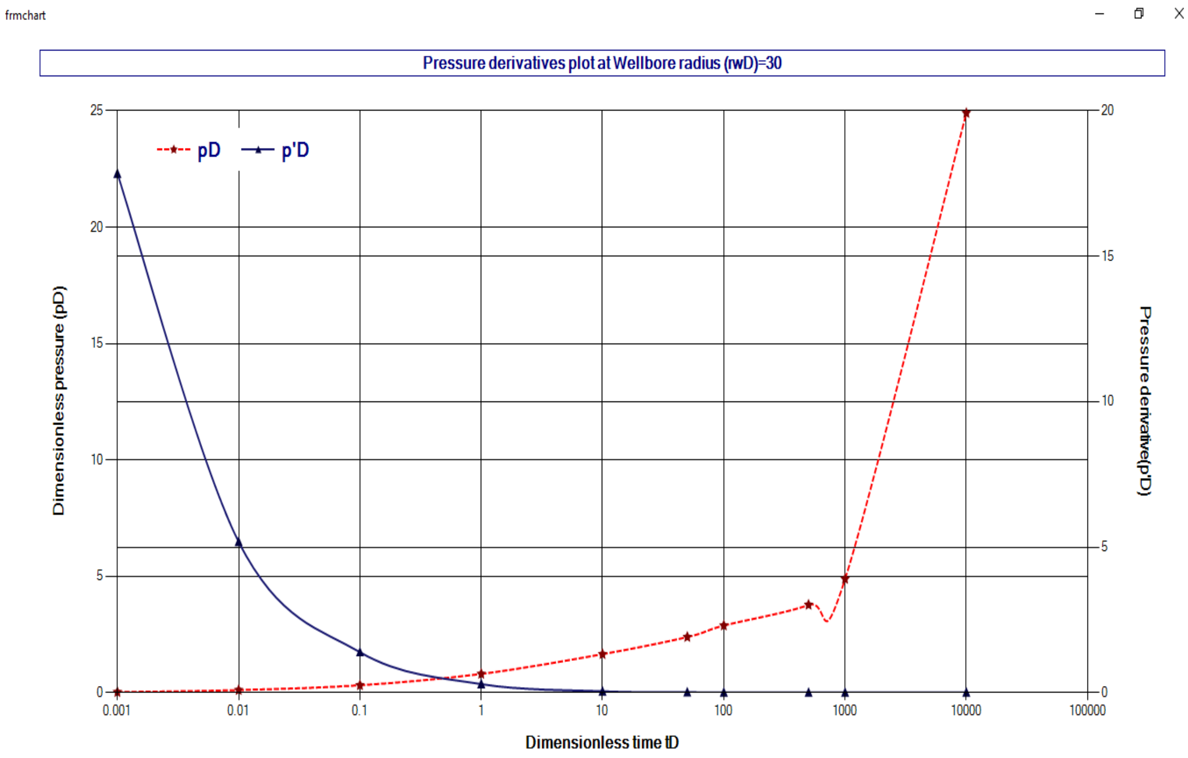

Fig. 7 *Dimensionless pressure and pressure derivative semi-log plot at r_{wD}=30*

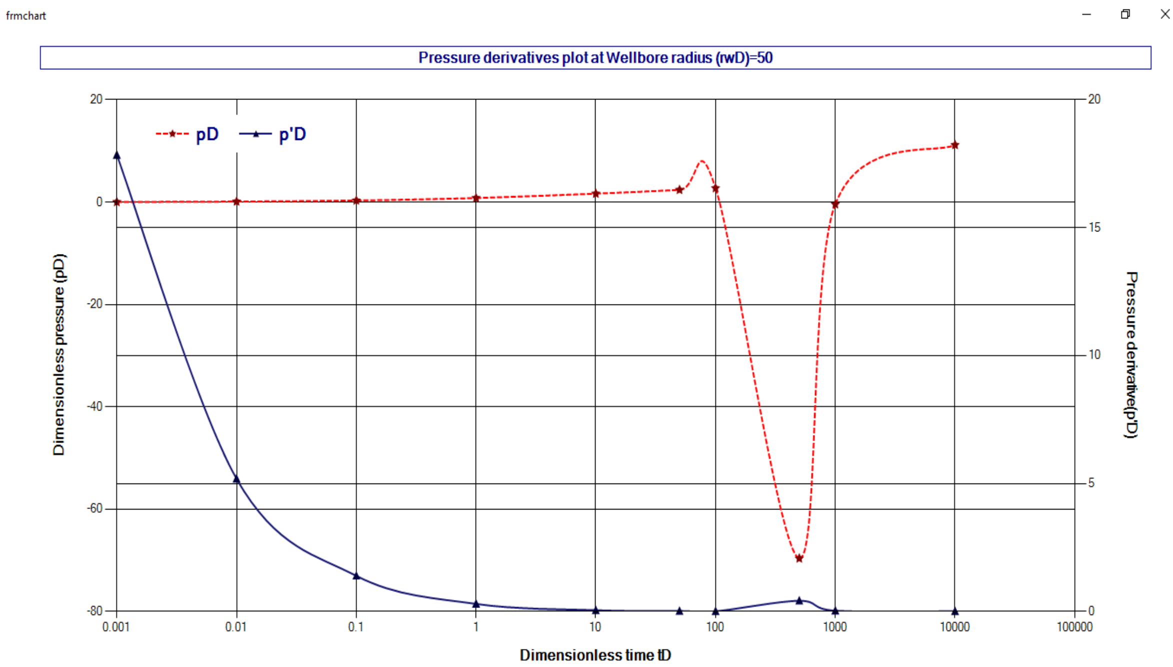

Fig. 8 *Dimensionless pressure and pressure derivative semi-log plot at r_{wD}=50*

The values of P_D became so low that it hits negative at dimensionless times greater than 100. At t_D=1000, a spike was observed in P_D as can be seen in Fig. 8. This spike is indicative that pressure derivatives and dimensionless variable are very sensitive to dimensionless time (t_D) values. Pressure derivative value, P'_D, also became negative at

t_D=1000 and became positive at t_D=10,000. Thus, reiterating the sensitivity of pressure derivatives to dimensionless time. Surprisingly, at wellbore radius of 100, no negative values were obtained for both dimensionless pressure, P_D and pressure derivative P'_D (refer to Fig. 9 for visual representation)

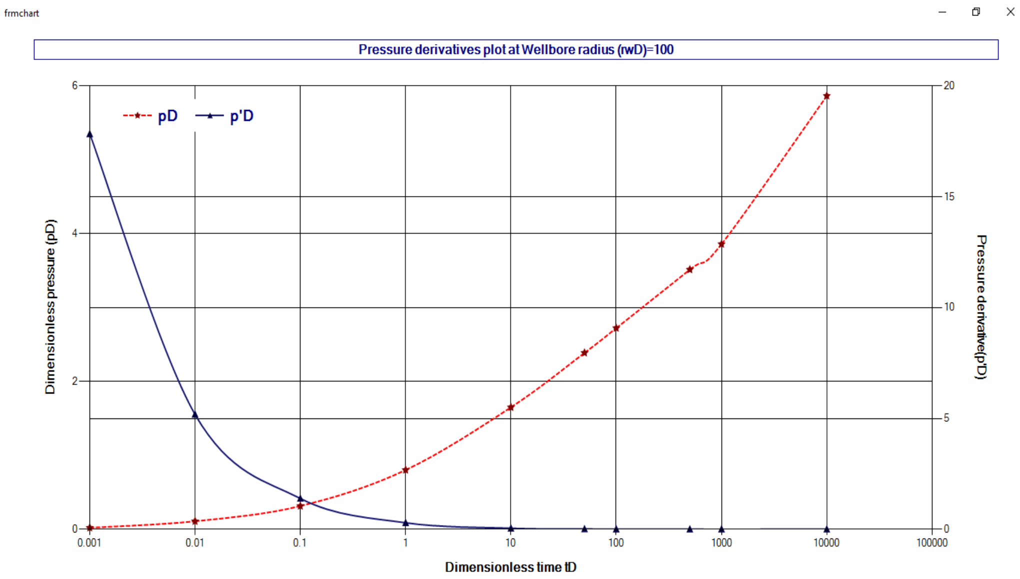

Fig. 9 *Dimensionless pressure and pressure derivative semi-log plot at r_{wD}=100*

Results for sensitivity analysis with diverse r_{wD} at fixed t_D

In this study, a range of dimensionless wellbore radii were examined at a fixed value of dimensionless time, so as to investigate their influence on pressure derivatives. This investigation was termed "sensitivity analysis". Thirty random wellbore radii (starting from 5.0 and terminating at 125) were examined at a fixed dimensionless time of 0.001. The result of this investigation is shown in a semi-log plot of pressure derivative and of P_D against wellbore radius as shown in Fig. 10.

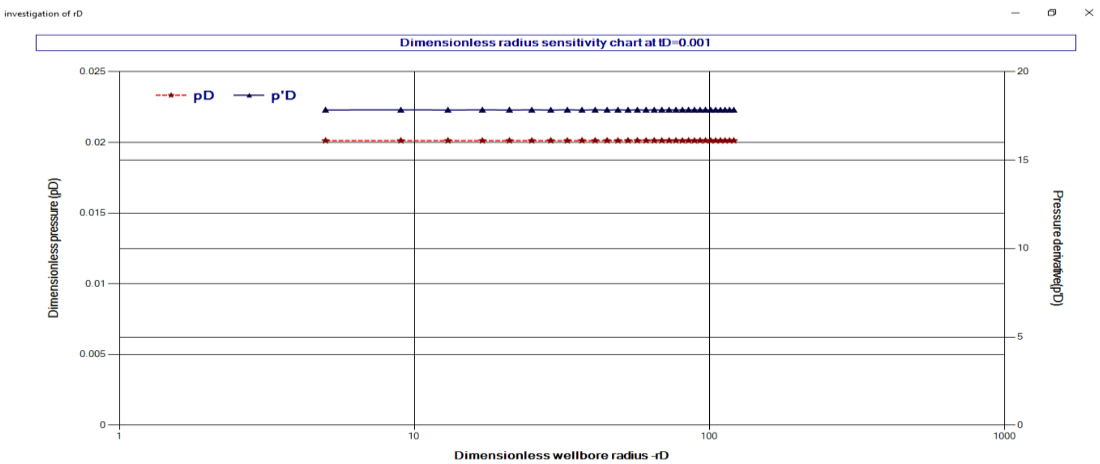

Fig. 10 *Dimensionless wellbore radius sensitivity chart at t_D=0.001*

The values of P_D and P'_D were estimated as 0.1081 and 5.1811 respectively at t_D=0.01 as seen in Fig. 11. Also, these values were observed to remain constant regardless of increase in r_{wD}. At t_D=0.5, P_D and P'_D values were calculated as 1.3783 and 0.09331 respectively.

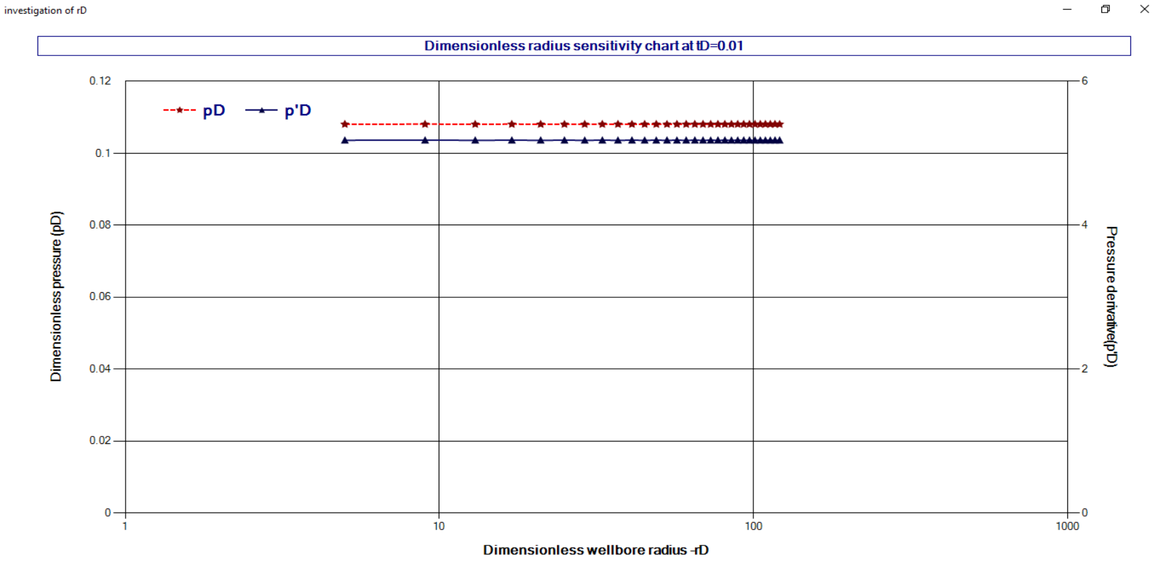

Fig. 11 *Dimensionless wellbore radius sensitivity chart at t_D=0.01*

Again, these values remained unchanged (just like the plot at t_D=0.001) despite the wide range of wellbore radii that were considered as seen in Fig. 12.

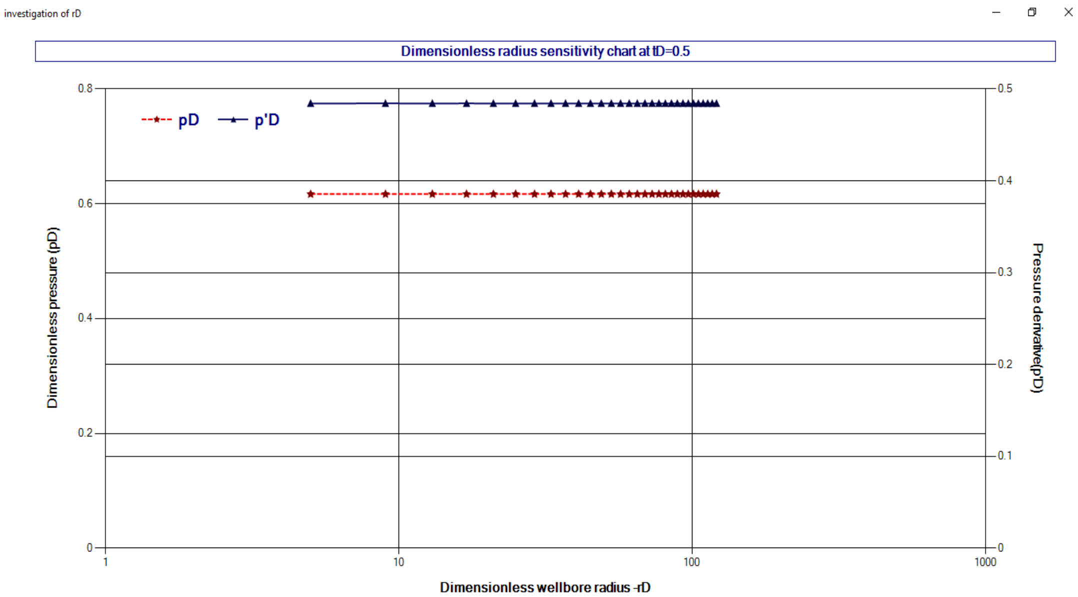

Fig. 12 *Dimensionless wellbore radius sensitivity chart at t_D=0.5*

At t_D=5, it was observed that the values of P_D and P'_D declined at a dimensionless wellbore radius of 9 and thereafter, remained constant with increase in the value of wellbore radius. This trend is illustrated in Fig. 13. This behaviour is reflective of the fact that at values of dimensionless time greater than 1, small values of dimensionless wellbore radius tend to influence pressure derivatives by increasing their value. It therefore implies that small wellbore radius results in high values of P_D and P'_D, thus, increasing the strength of the underground aquifer driving the vertical oil well. Likewise, at t_D values of 10, 20, 30 and 100, it was observed that P_D and P'_D decreased at wellbore radius of 9 then maintained constant values of P_D and P'_D at higher wellbore radius.

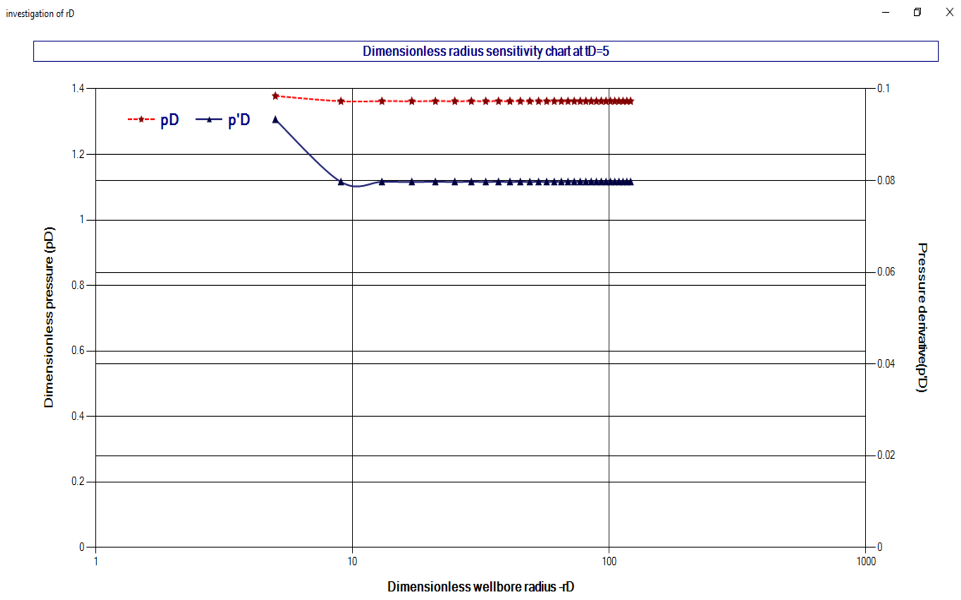

Fig. 13 *Dimensionless wellbore radius sensitivity chart at* t_D*=5*

Fig. 14, Fig. 15, Fig. 16 and Fig. 17 shows the sensitivity plots at fixed t_D of 10, 20, 30 and 100 respectively. It was noticed that higher dimensionless time caused steeper decrease in pressure derivatives between r_{wD} of 5 and 9.

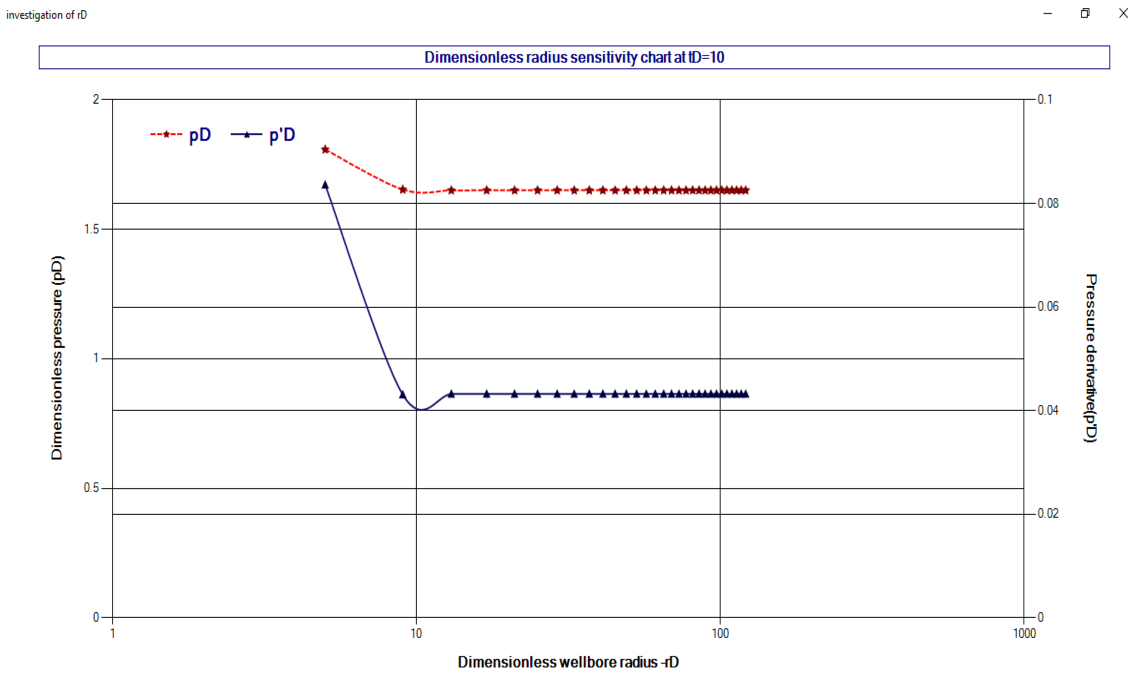

Fig. 14 *Dimensionless wellbore radius sensitivity chart at* t_D*=10*

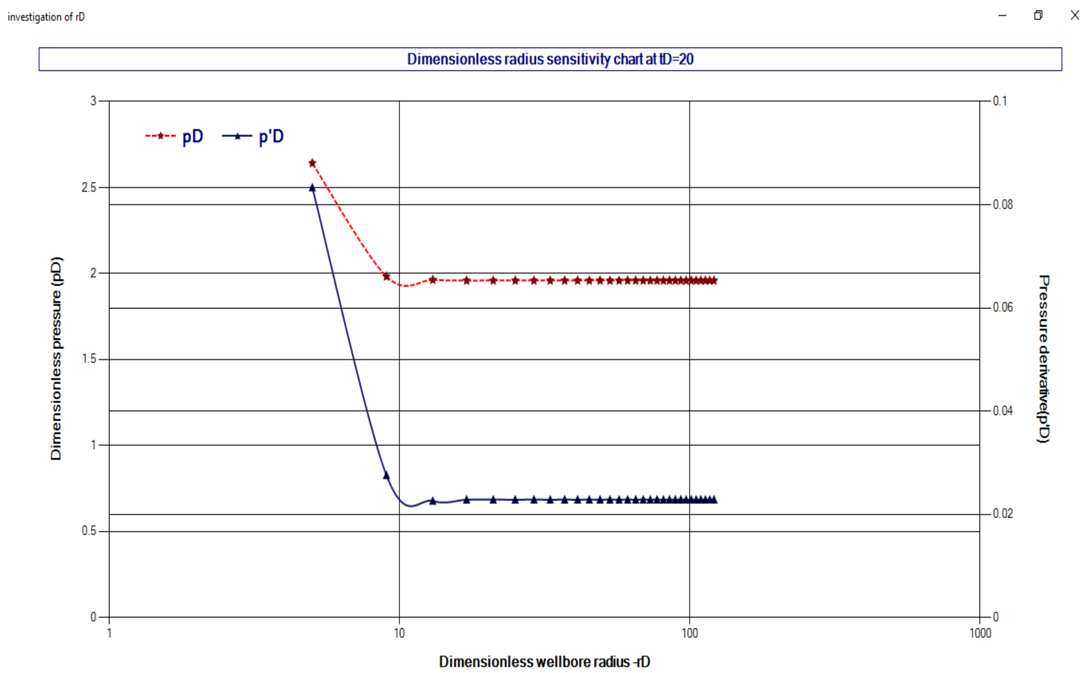

Fig. 15 *Dimensionless wellbore radius sensitivity chart at* t_D*=20*

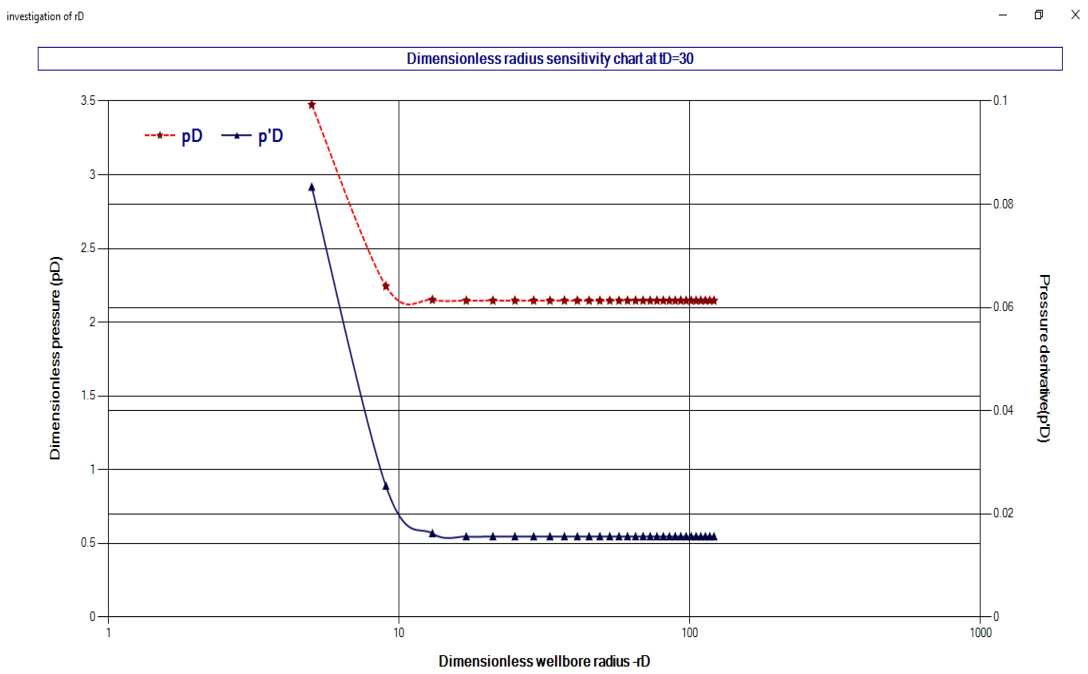

Fig. 16 *Dimensionless wellbore radius sensitivity chart at* t_D*=30*

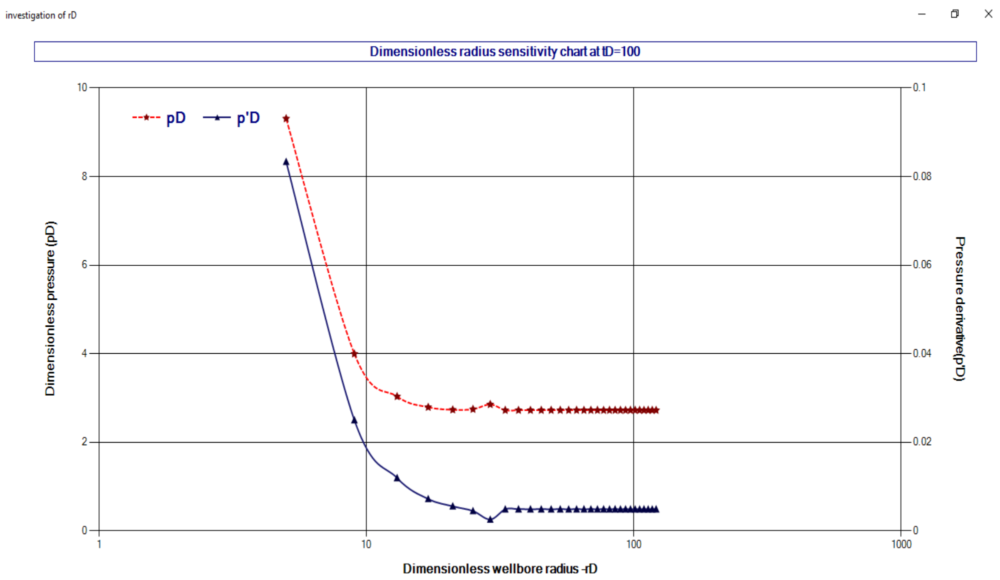

Fig. 17: *Dimensionless wellbore radius sensitivity chart at t_D=100*

Fig. 17 shows a sensitivity chart at t_D=100. The sharp decrease in pressure derivatives between r_{wD} =5 and r_{wD} =9, can be seen clearly, while Fig. 18 shows the calculated P_D and P'_D variables as performed by the developed computer model (EXPLORE).

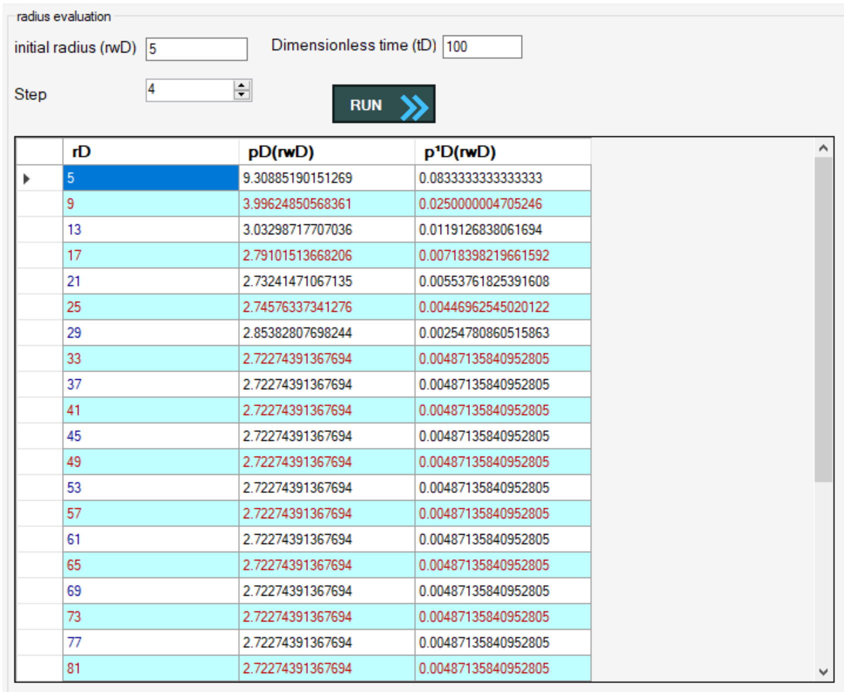

rD	pD(rwD)	p'D(rwD)
5	9.30885190151269	0.0833333333333333
9	3.99624850568361	0.0250000004705246
13	3.03298717707036	0.0119126838061694
17	2.79101513668206	0.00718398219661592
21	2.73241471067135	0.00553761825391608
25	2.74576337341276	0.00446962545020122
29	2.85382807698244	0.00254780860515863
33	2.72274391367694	0.00487135840952805
37	2.72274391367694	0.00487135840952805
41	2.72274391367694	0.00487135840952805
45	2.72274391367694	0.00487135840952805
49	2.72274391367694	0.00487135840952805
53	2.72274391367694	0.00487135840952805
57	2.72274391367694	0.00487135840952805
61	2.72274391367694	0.00487135840952805
65	2.72274391367694	0.00487135840952805
69	2.72274391367694	0.00487135840952805
73	2.72274391367694	0.00487135840952805
77	2.72274391367694	0.00487135840952805
81	2.72274391367694	0.00487135840952805

Fig. 18 *Dimensionless wellbore radius sensitivity variables calculations at t_D=100*

Result validation

By integrating some inputs of dimensionless radius and time, results from an Klins *et al.* [10] were used to validate the results produced by the software. Subsequently, the results from the developed software using the same inputs were compared analytically. Subsequently, the percentage error was computed by finding the difference between the two results and dividing the output by the published result (assumed to be the true value). Results obtained from this analysis for dimensionless pressure and pressure derivative are presented in Table 1 and Table 2, respectively. Invariably, the percentage errors computed were less than 0.02% for both P_D and P'_D. This reveals that the results obtained from the developed toolkit (EXPLORE) are very reliable.

Table 1 *Error analysis for dimensionless pressure calculations performed by EXPLORE.*

t_D	r_{wD}	P_D (published)	P_D (computed)	%Error
20	10	1.969	1.9691	0.005079
20	15	1.9589	1.9592	0.015315

Table 2 *Error analysis for pressure derivative calculations performed by EXPLORE*

t_D	r_{wD}	P'_D (published)	P'_D (computed)	%Error
20	10	0.0247	0.02475	0.20242915
20	15	0.0228	0.0228	0

CONCLUSION

This study has examined the influence of dimensionless wellbore radius on dimensionless pressure and pressure derivatives. These pressure variables help define the productivity of oil wells. This research focused on vertical oil wells. Pressure derivatives were calculated using Van-Everdingen aquifer models. EXPLORE was developed as software that analyzes pressure derivatives based on dimensionless time and wellbore radius. The software applies the correlations for infinitely acting and finitely acting aquifers. The study results show that a low dimensionless wellbore radius increases pressure derivative values, indicating high well productivity. High-pressure derivatives suggest the aquifer can move oil from the reservoir's pore throat to the wellbore. Sensitivity analysis was performed with different values of wellbore radius (rWD) using a fixed value of dimensionless time to examine the influence of rWD on dimensionless pressure, and pressure derivatives show that pressure derivatives peaked at less than 10 dimensionless wellbore radius.

Nonetheless, at rWD greater than ten, the values of pressure derivative (P'D) and dimensionless pressure (PD) remained constant regardless of the increase in dimensionless wellbore radius (rWD). Higher dimensionless time values causes steeper trends (greater pressure derivative drops) from the lowest dimensionless radius for both PD and P'D. To conclude, error analysis was performed on the EXPLORE software results to validate the accuracy. The results were compared with Klins *et al.* [10] and had a percentage error of less than 0.02%, which is considered acceptable.

REFERENCES

[1] Eiroboyi, I., Wilkie, S.I., Comparative evaluation of pressure distribution between horizontal and vertical wells in a reservoir (Edge water drive). *Nigerian Journal of Technology*, 36(2), pp 457-460, 2017.

[2] Ahmed, T., McKinney, P., *Advanced reservoir engineering*. Elsevier. 2011.

[3] Ju, B., Dai, S., Fan, T., Wang, X., Wu, H., An effective method to improve recovery of heavy oil reservoir with bottom water drive. In *International Petroleum Technology Conference*. OnePetro, 2005.

[4] Naderi, M., Rostami, B., Khosravi, M., Effect of heterogeneity on the productivity of vertical, deviated and horizontal wells in water drive gas reservoirs. *Journal of Natural Gas Science and Engineering*, 23, pp 481-491, 2015.

[5] Sharma, P., Kumar, M., Gupta, D.K., 3D numerical simulation of clastic reservoir with bottom water drive using various ior techniques for maximizing recovery. *Journal of Petroleum Exploration and Production Technology*, 9(2), pp 1075-1087, 2019.

[6] Oloro, J.O., Adewole, S.E., Performance and behavior of a horizontal well in reservoir subject to double-edged water drive. *Nigerian Journal of Technology*, 39(2), pp 417-423, 2020.

[7] Adewole, E.S., Olafuyi, O.A., The use of source and Green's functions to derive dimensionless pressure and dimensionless pressure derivative distribution of a two-layered reservoir Part I: A-Sha ed Architecture. *Journal of Mathematics and Technology*, pp 92-101, 2010.

[8] Eiroboyi, I., Adewole, E.S., Type Curves for a Reservoir Subject to Active Bottom Water Drive. In *Advanced Materials Research*, Vol. 824, pp. 373-378 Trans Tech Publications Ltd., 2013.

[9] Edobhiye, O., Adewole, E.S., Effects of Both Wellbore and Reservoir Properties on Dimensionless Pressure and Dimensionless Pressure Derivative Distribution of a Horizontal Well in a Reservoir Subject to Bottom Water, Gas Cap and Single Edge Water Drive Mechanisms. In *SPE Nigeria Annual International Conference and Exhibition*. OnePetro, 2014.

[10] Klins, M.A., Bouchard, A.J., Cable, C.L., A polynomial approach to the van Everdingen-Hurst dimensionless variables for water encroachment. *SPE Reservoir Engineering*, 3(01), 320-326, 1988.

Received: January 2023; Accepted: February 2023; Published: February 2023